Hindawi Publishing Corporation
Shock and Vibration
Volume 2014, Article ID 284367, 15 pages
http://dx.doi.org/10.1155/2014/284367

Research Article

Mobility Matrix of a Thin Circular Plate Carrying Concentrated Masses Based on Transverse Vibration Solution

Desheng Li and Junhong Zhang

State Key Laboratory of Engines, Tianjin University, Weijin Road 92, Tianjin 300072, China

Correspondence should be addressed to Desheng Li; lidesh@tju.edu.cn

Received 30 November 2013; Accepted 6 July 2014; Published 7 August 2014

Academic Editor: Kumar V. Singh

When calculating the vibration or sound power of a vibration source, it is necessary to know the point mobility of the supporting structure. A new method is presented for the calculation of point mobility matrix of a thin circular plate with concentrated masses in this paper. Transverse vibration mode functions are worked out by utilizing the structural circumferential periodicity of the inertia excitation produced by the concentrated masses. The numerical vibratory results, taking the clamped case as an instance, are compared to the published ones to validate the method for ensuring the correctness of mobility solution. Point mobility matrix, including the driving and transfer point mobility, of the titled structure is computed based on the transverse vibration solution. After that, effect of the concentrated masses on the mechanical point mobility characteristics is analyzed.

1. Introduction

Design of quiet and low vibration equipment requires quantitative data of the sound and vibration sources. Mechanical point mobility matrix is an appropriate tool to describe the dynamic characteristics and is needed for the estimation of vibration and sound power transmission from the source to the receiving structure if the energy based methods are used. In many cases, it is impossible to measure the point mobility needed for an analysis directly; therefore, it is necessary to calculate them in terms of the relative theory.

Much work has been done in finding analytical formula for point mobility. Fahy [1], Fahy and Gradonio [2] and Cremer et al. [3] gave a comprehensive summary of formulas for kinds of classical structures, such as beams, plates, and shells. Many authors, among them Sarradj [4], Moorhouse and Gibbs [5], Bonhoff and Petersson [6], and Mayr and Gibbs [7], calculated various point mobility of beam/plate-like components in more or less detail. In contrast, more results of point mobility were applied in complicated and built-up structures. Petersson and Heckl [8] studied point mobility for the plate with arbitrary thickness and the deep beams. Sciulli [9] analyzed the true effects of vibrating system flexibility. Grice and Pinnington [10] estimated the mean-square flexural vibration of a thin plate box via calculating its mechanical impedances. Putra [11] modified Laulegnat's model by applying impedance and mobility to research the sound radiation of a perforated plate. Wang [12] provided a general formula to solve the vibration problem for continuous systems. Yun and Mak [13] reported the effects of the interaction between two vibratory machines on the power transmitted to a coupling dual-layered floor plate and the level of power transmissibility by simulating the floor structure mobility. Zu and Mak [14] proposed a method to determine the best mounting position for isolated vibratory equipment in buildings by obtaining the floor mobility at all possible positions. Huang et al. [15] presented a systematic modeling method to analyze the vibration transmission of a typical floating raft system in submarines according to the mobility calculation. Chen and Wu [16] established a model of a base system consisting of two isolators and a beam to calculate the force transfer rate by adopting the transfer matrix method.

The most common ground in the previous research is that the subjects investigated are always homogeneous beam, plate, and shell. However, most components are not the case in actual project. Additional structures, such as concentrated mass, oscillator, and interior support, are attached to the components and the case in which the plates with variable thickness or tapered indentations [17, 18] are also being

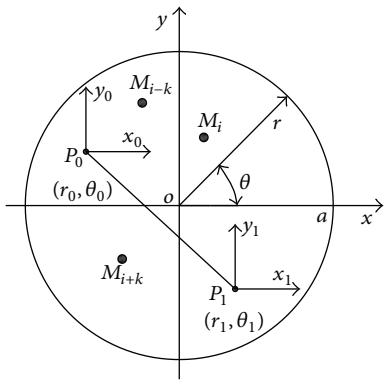

Figure 1: Sign convention and coordinates systems of thin circular plate with concentrated masses.

involved. In this paper, point mobility function of a thin circular plate carrying concentrated masses with simple boundary conditions, including simply supported, clamped and free outer boundaries, is studied. Firstly, the transverse vibration mode functions are computed utilizing the structural circumferential periodicity of the inertia excitation produced by the concentrated masses and the numerical results are compared to the existing ones calculated by using the other mature technology. And, then, the mobility matrix consists of the force and moment and coupling mobility is worked out according to the methodology in [19]. Finally, the clamped case was taken as an instance to describe the influence of the mass parameters on the point mobility characteristics.

2. Solution of Transverse Vibration

Solution of mode functions is a principal and pivotal link in point mobility calculation of the elastic continuum. In this section, a mathematical model utilizing the structural circumferential periodicity produced by the concentrated masses will be established to describe the free transverse vibration of the titled structure. The numerical vibratory results will be compared to the ones generated from the other methods to validate the presented mathematical model and to ensure the correctness of the point mobility calculation.

2.1. Governing Differential Equation. Figure 1 is an isotropic thin circular plate carrying concentrated masses M_i, whose position is (r_i, θ_i) when the cylindrical coordinates of reference (r, θ, z) are located at the center with the z-axis orthogonal to the surface of the plate and coincide with the z-axis of the Cartesian coordinate system (o, x, y, z).

The governing differential equation of the transverse vibration can be written according to the classical plate theory:

$$D\nabla^2\nabla^2 w(r,\theta,t) + \rho h \frac{\partial^2}{\partial t^2} w(r,\theta,t) = p(r,\theta,t), \quad (1)$$

where $D = Eh^3/[(1-v^2)]$ is the bending stiffness, E is Young's modulus, h is the plate thickness, v is Poisson's ratio,

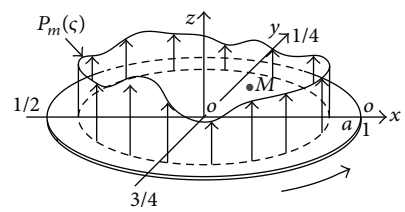

Figure 2: Diagrammatic sketch of the structural circumferential periodicity of transverse shearing stress.

∇^2 is the Laplacian operator, w is the transverse displacement, ρ is mass density, and p is inertia excitation produced by the concentrated masses. Since the system motion can be regarded as a simple harmonic vibration, the transverse displacement and the inertia excitation may be assumed as follows:

$$w(r,\theta,t) = W(r,\theta)\, e^{j\omega t}, \quad (2a)$$

$$p(r,\theta,t) = P(r,\theta)\, e^{j\omega t}, \quad (2b)$$

where ω denotes the natural frequency, $j = \sqrt{-1}$, and W is the natural mode of the plate. For convenience in later mathematical work, the following dimensionless parameters are introduced:

$$\varsigma = \frac{r}{a}, \quad (3a)$$

$$\varsigma_i = \frac{r_i}{a}, \quad (3b)$$

$$\eta = \theta, \quad (3c)$$

$$\eta_i = \theta_i, \quad (3d)$$

where r and θ are the polar radius and polar angle of an arbitrary point on plate, respectively, a is the radius of the plate, and the subscript i represents the serial number of concentrated masses. Substituting the dimensionless parameters above into (1), the expression could be deduced:

$$D\nabla^2\nabla^2 W(\varsigma,\eta) - \lambda^4 W(\varsigma,\eta) = \sum_{i=1}^{N} P_i(\varsigma_i,\eta_i), \quad (4)$$

where P_i is the excitation force amplitude generated at the masses' position (ς_i, η_i) and λ is the fundamental frequency coefficient and is defined by

$$\lambda^4 = \frac{\rho h}{D} a^4 \omega^2. \quad (5)$$

The structural circumferential periodicity of the inertial excitation is shown in Figure 2. The inertia excitation will make the whole plate with transverse shearing stress, whose value is various at different positions. If we start a concentric circle from any angle through the stress change process, it can be found that the stress value at the finished point equals

the value where the circle starts. This kind of periodicity does exist and is available. In this section, the structural circumferential periodicity will be utilized to establish a new mathematical model and to calculate the transverse free vibration characteristics.

When the structure vibrates freely, the frequency of the force P is consistent with the natural frequency of the structure. Thus, the transverse displacement amplitude and the inertia excitation can be assumed as follows:

$$W(\varsigma,\eta) = \sum_{m=1}^{\infty} R_m(\varsigma)\cos(m\eta), \tag{6a}$$

$$P(\varsigma,\eta) = \sum_{m=1}^{\infty} P_m(\varsigma)\cos(m\eta). \tag{6b}$$

Substituting (6a) and (6b) into (4) yields

$$\left(\frac{d^2}{d^2\varsigma}+\frac{1}{\varsigma}\frac{d}{d\varsigma}-\frac{m^2}{\varsigma^2}\right)\left(\frac{d^2}{d^2\varsigma}+\frac{1}{\varsigma}\frac{d}{d\varsigma}-\frac{m^2}{\varsigma^2}\right)R_m(\varsigma) - \lambda^4 R_m(\varsigma) = \frac{P_m(\varsigma)}{D}. \tag{7}$$

Solution of (7) can be obtained and written as

$$\begin{aligned} R_m(\varsigma) &= A_1 J_m(\lambda\varsigma) + A_2 Y_m(\lambda\varsigma) \\ &\quad + A_3 I_m(\lambda\varsigma) + A_4 K_m(\lambda\varsigma) + \frac{\varepsilon_m \pi}{4D\lambda^2} \\ &\quad \times \int_0^{\varsigma} P_m(s)\left\{J_m(\lambda\varsigma)Y_m(\lambda s) - Y_m(\lambda\varsigma)J_m(\lambda s)\right. \\ &\qquad \left. + \frac{2}{\pi}\left[I_m(\lambda\varsigma)K_m(\lambda s) - K_m(\lambda\varsigma)I_m(\lambda s)\right]\right\} s\,ds. \end{aligned} \tag{8}$$

The former 4 terms on the right of the equation are the general solution of homogeneous Kamke differential equation and the last integral term is the particular solution of the nonhomogeneous equation. J_m and Y_m are the Bessel functions of the first and second kinds and I_m and K_m are modified Bessel functions of the first and second kinds, respectively. The integral coefficients $A_1 \sim A_4$ determine the mode shape and can be solved from the boundary conditions. The coefficient ε_m is given by

$$\varepsilon_m = \begin{cases} 0.5, & m = 0, \\ 1, & m \geq 1. \end{cases} \tag{9}$$

2.2. Integral Constants. The integral coefficients $A_1 \sim A_4$ in (8) can be determined by the structure and boundary conditions. When the origin of cylindrical coordinates system is taken to coincide with the center of the circular plate and no internal holes attached to the plate are considered, the terms of (8) involving Y_m and K_m terms must be discarded in order to avoid the infinite deflections and stresses at the plate center where $r = 0$:

$$A_2 = A_4 = 0. \tag{10}$$

Substituting (10) into (8), the expression under simple boundary conditions could be deduced as follows:

$$\begin{aligned} R_m(\varsigma) &= A_1 J_m(\lambda\varsigma) + A_3 I_m(\lambda\varsigma) + \frac{\varepsilon_m \pi}{4D\lambda^2} \\ &\quad \times \int_0^{\varsigma} P_m(s)\left\{J_m(\lambda\varsigma)Y_m(\lambda s) - Y_m(\lambda\varsigma)J_m(\lambda s)\right. \\ &\qquad \left. + \frac{2}{\pi}\left[I_m(\lambda\varsigma)K_m(\lambda s) - K_m(\lambda\varsigma)I_m(\lambda s)\right]\right\} s\,ds, \end{aligned} \tag{11}$$

$$A_1 = \frac{\varepsilon_m \pi}{4D\lambda^2} \times \int_0^{a} P_m(s)\left\{G_1 J_m(\lambda s) - Y_m(\lambda s) + \frac{2}{\pi}G_2 I_m(\lambda s)\right\} s\,ds, \tag{12a}$$

$$A_3 = \frac{\varepsilon_m \pi}{4D\lambda^2} \times \int_0^{a} P_m(s)\left\{G_3 J_m(\lambda s) + \frac{2}{\pi}\left[G_4 I_m(\lambda s) - K_m(\lambda s)\right]\right\} s\,ds. \tag{12b}$$

For a simple supported circular plate, the calculation of $G_1 \sim G_4$ is

$$G_1 = \frac{\left[S_3 Y_m(\lambda a) - S_2 I_m(\lambda a)\right]}{\Theta_S}, \tag{13a}$$

$$G_2 = \frac{\left[S_3 K_m(\lambda a) - S_4 I_m(\lambda a)\right]}{\Theta_S}, \tag{13b}$$

$$G_3 = \frac{\left[S_2 J_m(\lambda a) - S_1 Y_m(\lambda a)\right]}{\Theta_S}, \tag{13c}$$

$$G_4 = \frac{\left[S_4 J_m(\lambda a) - S_1 K_m(\lambda a)\right]}{\Theta_S}, \tag{13d}$$

$$\Theta_S = S_3 J_m(\lambda a) - S_1 I_m(\lambda a), \tag{13e}$$

where $S_1 \sim S_4$ are defined:

$$S_1 = \ddot{J}_m(\lambda a) + \frac{\mu}{a}\left[\dot{J}_m(\lambda a) - \frac{m^2}{a}J_m(\lambda a)\right], \tag{14a}$$

$$S_2 = \ddot{Y}_m(\lambda a) + \frac{\mu}{a}\left[\dot{Y}_m(\lambda a) - \frac{m^2}{a}Y_m(\lambda a)\right], \tag{14b}$$

$$S_3 = \ddot{I}_m(\lambda a) + \frac{\mu}{a}\left[\dot{I}_m(\lambda a) - \frac{m^2}{a}I_m(\lambda a)\right], \tag{14c}$$

$$S_4 = \ddot{K}_m(\lambda a) + \frac{\mu}{a}\left[\dot{K}_m(\lambda a) - \frac{m^2}{a}K_m(\lambda a)\right]. \tag{14d}$$

For clamped case, the calculation of $G_1 \sim G_4$ is

$$G_1 = \frac{\left[\dot{I}_m(\lambda a) Y_m(\lambda a) - I_m(\lambda a) \dot{Y}_m(\lambda a)\right]}{\Theta_C}, \tag{15a}$$

$$G_2 = \frac{\left[\dot{I}_m(\lambda a) K_m(\lambda a) - I_m(\lambda a) \dot{K}_m(\lambda a)\right]}{\Theta_C}, \tag{15b}$$

$$G_3 = \frac{\left[J_m(\lambda a) \dot{Y}_m(\lambda a) - \dot{J}_m(\lambda a) Y_m(\lambda a)\right]}{\Theta_C}, \tag{15c}$$

$$G_4 = \frac{\left[J_m(\lambda a) \dot{K}_m(\lambda a) - \dot{J}_m(\lambda a) K_m(\lambda a)\right]}{\Theta_C}, \tag{15d}$$

$$\Theta_C = J_m(\lambda a) \dot{I}_m(\lambda a) - I_m(\lambda a) \dot{J}_m(\lambda a). \tag{15e}$$

For free case, the calculation of $G_1 \sim G_4$ is

$$G_1 = \frac{\left[S_2 T_3(\lambda a) - S_3 T_2(\lambda a)\right]}{\Theta_F}, \tag{16a}$$

$$G_2 = \frac{\left[S_4 T_3(\lambda a) - S_3 T_4(\lambda a)\right]}{\Theta_F}, \tag{16b}$$

$$G_3 = \frac{\left[S_1 T_2(\lambda a) - S_2 T_1(\lambda a)\right]}{\Theta_F}, \tag{16c}$$

$$G_4 = \frac{\left[S_1 T_4(\lambda a) - S_4 T_1(\lambda a)\right]}{\Theta_F}, \tag{16d}$$

$$\Theta_F = S_1 T_3(\lambda a) - S_3 T_1(\lambda a). \tag{16e}$$

Here,

$$T_1(\lambda a) = \left\{\frac{d}{dr}\left[\ddot{J}_m(\lambda r) + \frac{\dot{J}_m(\lambda r)}{r} - \frac{m^2 J(\lambda r)}{r^2}\right] + \frac{m^2(1-\mu)}{r^2}\left[\frac{J_m(\lambda r)}{r} - \dot{J}_m(\lambda r)\right]\right\}_{r=a}, \tag{17a}$$

$$T_2(\lambda a) = \left\{\frac{d}{dr}\left[\ddot{Y}_m(\lambda r) + \frac{\dot{Y}_m(\lambda r)}{r} - \frac{m^2 Y(\lambda r)}{r^2}\right] + \frac{m^2(1-\mu)}{r^2}\left[\frac{Y_m(\lambda r)}{r} - \dot{Y}_m(\lambda r)\right]\right\}_{r=a}, \tag{17b}$$

$$T_3(\lambda a) = \left\{\frac{d}{dr}\left[\ddot{I}_m(\lambda r) + \frac{\dot{I}_m(\lambda r)}{r} - \frac{m^2 I(\lambda r)}{r^2}\right] + \frac{m^2(1-\mu)}{r^2}\left[\frac{I_m(\lambda r)}{r} - \dot{I}_m(\lambda r)\right]\right\}_{r=a}, \tag{17c}$$

$$T_4(\lambda a) = \left\{\frac{d}{dr}\left[\ddot{K}_m(\lambda r) + \frac{\dot{K}_m(\lambda r)}{r} - \frac{m^2 K(\lambda r)}{r^2}\right] + \frac{m^2(1-\mu)}{r^2}\left[\frac{K_m(\lambda r)}{r} - \dot{K}_m(\lambda r)\right]\right\}_{r=a}. \tag{17d}$$

2.3. Inertia Excitation. When the structure in Figure 1 vibrates freely, the inertia force of the concentrated masses can be regarded as a kind of excitation. The forcing function can be written as

$$P(\varsigma, \eta) = \sum_{i=1}^{N} \frac{P_{m,i}}{2a\pi} \delta(\varsigma - \varsigma_i) \delta(\eta - \eta_i), \tag{18}$$

where $P_{m,i}$ is the amplitude of the inertia force produced by the ith mass which position is (ς_i, η_i) and δ is the Dirac delta function.

The right side of (18) can be expanded into Fourier-Bessel series with functions $J_m(x)$ and $\cos(m\eta)$. So, (18) could be expressed then as

$$P(\varsigma, \eta) = \sum_{m,n}^{\infty} \varepsilon_m \sum_{i=1}^{N} P_{mn,i} J_m\left(\lambda_n^{(m)} \varsigma\right) \cos(m\eta), \tag{19}$$

where $\lambda_n^{(m)}$ is the nth positive root of the Bessel function $J_m(x) = 0$.

Comparing to (6b), the structural circumferential periodicity can be formulated as follows:

$$P_m(\varsigma) = \sum_{n}^{\infty} \varepsilon_m \sum_{i}^{N} P_{mn,i} J_m\left(\lambda_n^{(m)} \varsigma\right). \tag{20}$$

Calculation of $P_{mn,i}$ can be performed as

$$P_{mn,i} = \frac{2P_{m,i}}{\pi} \frac{J_m\left(\lambda_n^{(m)} \varsigma_i\right)}{J_{m+1}^2\left(\lambda_n^{(m)}\right)} \cos(m\eta_i), \tag{21a}$$

$$P_{m,i} = M_i \omega^2 W(\varsigma_i, \eta_i). \tag{21b}$$

Substituting (21a) and (21b) into (11), the displacements and mode functions can be formulated as

$$R_m(\varsigma) = \frac{\varepsilon_m \pi}{4D\lambda^2} \sum_{i=1}^{N} P_{m,i} \varsigma_i \left[B_1 J_m(\lambda\varsigma) + B_3 I_m(\lambda\varsigma) + C_i U_i(\varsigma - \varsigma_i)\right] \cos(m\pi\eta_i), \tag{22}$$

$$W(\varsigma, \eta) = \sum_{m=1}^{\infty} R_m(\varsigma) \cos(m\eta). \tag{23}$$

Here,

$$B_1 = G_1 J_m(\lambda\varsigma_i) - Y_m(\lambda\varsigma_i) + \frac{2}{\pi} G_2 I_m(\lambda\varsigma_i),$$
$$B_3 = G_3 J_m(\lambda\varsigma_i) - \frac{2}{\pi} K_m(\lambda\varsigma_i) + \frac{2}{\pi} G_4 I_m(\lambda\varsigma_i), \tag{24a}$$

$$C_i = J_m(\lambda\varsigma_i) Y_m(\lambda\varsigma_i) - Y_m(\lambda\varsigma_i) J_m(\lambda\varsigma_i) + \frac{2}{\pi}\left[I_m(\lambda\varsigma_i) K_m(\lambda\varsigma_i) - K_m(\lambda\varsigma_i) I_m(\lambda\varsigma_i)\right], \tag{24b}$$

$$U_i(\varsigma - \varsigma_i) = \begin{cases} 1 & \varsigma > \varsigma_i \\ 0 & \varsigma < \varsigma_i. \end{cases} \tag{24c}$$

U_i is the step function. The mathematical model is appropriate to the case that the concentrated masses locate at the eccentric position. For the center case, refer to Leissa [20].

2.4. Frequency Equation. According to (21b), the inertia excitation of the jth concentrated mass can be formulated as

$$P_{m,j} = M_j \omega^2 W\left(\varsigma_j, \eta_j\right). \tag{25}$$

Substituting (23) into (21b), the homogeneous linear equations can be obtained as

$$\begin{bmatrix} Q_{11}+\Lambda_1 & Q_{12} & \cdots & Q_{1N} \\ Q_{21} & Q_{22}+\Lambda_2 & \cdots & Q_{2N} \\ \vdots & \vdots & \ddots & \vdots \\ Q_{N1} & Q_{N2} & \cdots & Q_{NN}+\Lambda_N \end{bmatrix} \begin{bmatrix} P_{m,1} \\ P_{m,2} \\ \vdots \\ P_{m,N} \end{bmatrix} = 0. \tag{26}$$

Calculation of the diagonal elements in (26) is

$$\begin{aligned} Q_{ij} = \sum_{m}^{\infty} \varsigma_j \left[B_1 J_m\left(\lambda \varsigma_j\right) + B_3 I_m\left(\lambda \varsigma_j\right) \right. \\ \left. + C_{ij} U_{ij}\left(\varsigma_i - \varsigma_j\right)\right] \cos\left(m\eta_i\right) \cos\left(m\eta_j\right). \end{aligned} \tag{27a}$$

Here,

$$\begin{aligned} C_{ij} = J_m\left(\lambda r_i\right) Y_m\left(\lambda r_j\right) - Y_m\left(\lambda r_i\right) J_m\left(\lambda r_j\right) \\ + \frac{2}{\pi}\left[I_m\left(\lambda r_i\right) K_m\left(\lambda r_j\right) - K_m\left(\lambda r_i\right) I_m\left(\lambda r_j\right)\right], \end{aligned} \tag{27b}$$

$$U_{ij}\left(r_i - r_j\right) = \begin{cases} 1 & r_i > r_j \\ 0 & r_i < r_j, \end{cases} \tag{27c}$$

$$\Lambda_i = \frac{-\left(2/\pi a \lambda\right)^2}{\psi_i}, \quad \psi_i = \frac{M_i}{\rho \pi a^2 h}. \tag{27d}$$

ψ_i is the ratio of the concentrated mass M_i to the circular plate M_P. Considering that all the solutions of (26) are nonzero, the natural frequency equation can be expressed as

$$\begin{vmatrix} Q_{11}+\Lambda_1 & Q_{12} & \cdots & Q_{1N} \\ Q_{21} & Q_{22}+\Lambda_2 & \cdots & Q_{2N} \\ \vdots & \vdots & \ddots & \vdots \\ Q_{N1} & Q_{N2} & \cdots & Q_{NN}+\Lambda_N \end{vmatrix} = 0. \tag{28}$$

The order of the determinant in (28) equals the number of the concentrated masses. Substitute the natural frequency solved from (28) into (21b) and combine the relative values with (23); the relative values of $P_{m,i}$ and the mode functions can be obtained.

3. Point Mobility Matrix Modeling

The structure shown in Figure 1 can be considered a linear and time invariant system, which is excited by a general force field $F\exp(i\omega t)$ expressed as complex force amplitude F times a harmonically varying function of time $\exp(i\omega t)$. Owing to the system linearity the corresponding general velocity field is also harmonic, $V\exp(i\omega t)$, and the ratio is independent of the amplitude of the exciting force. If the excitation is harmonic at angular frequency ω, the generalized mechanical mobility functions can be defined as follows:

$$Y = \frac{V}{F}. \tag{29}$$

Given the linear system in Figure 1 subjected to simultaneously acting force and moments excitations in the directions of z-, x-, and y-axes, respectively, the translational and rotational velocity responses at a certain position can be derived as follows:

$$\begin{Bmatrix} \dot{w} \\ \dot{\theta}_x \\ \dot{\theta}_y \end{Bmatrix} = \begin{bmatrix} Y_{11} & Y_{12} & Y_{13} \\ Y_{21} & Y_{22} & Y_{23} \\ Y_{31} & Y_{32} & Y_{33} \end{bmatrix} \begin{Bmatrix} F \\ M_x \\ M_y \end{Bmatrix}. \tag{30}$$

The diagonal elements in the matrix are the force and moment mobility functions, and the nondiagonal elements are the coupling mobility functions resulting from the simultaneously acting force and moment excitations.

3.1. Driving Point Mobility. For a thin circular plate carrying concentrated masses, the transverse displacement amplitude function at any point, due to a sinusoidal lateral load of $F(r_0, \theta_0)\sin\omega t$, is given by [3, 19]

$$w(r,\theta) = F \sum_{m=1}^{\infty}\sum_{n=1}^{\infty} \frac{W_{mn}(r,\theta)}{\left[\omega_{mn}^2(1+j\eta) - \omega^2\right] M_{mn}} W_{mn}(r_0,\theta_0), \tag{31}$$

where W_{mn} is the vibration mode function, ω_{mn} is the nature frequency, ω is the excitation frequency, and η is loss factor. Modal mass M_{mn} can be calculated as

$$M_{mn} = \rho h \iint_S W_{mn}^2(r,\theta)\, dS. \tag{32}$$

Here, S is the domain of the circular plate. According to the impedance transform theory (ITT), displacement expression of (31) can be transferred into velocity:

$$\begin{aligned} \dot{w}(x,y) \\ = j\omega F \sum_{m=1}^{\infty}\sum_{n=1}^{\infty} \frac{W_{mn}(r,\theta)}{\left[\omega_{mn}^2(1+j\eta) - \omega^2\right] M_{mn}} W_{mn}(r_0,\theta_0). \end{aligned} \tag{33}$$

The driving point mobility is the ratio of velocity response to the excitation force at the same point in the system. Thus, the force mobility can be written as

$$Y_{11} = \frac{\dot{w}_y(x_0,y_0)}{F} = j\omega \sum_{m=1}^{\infty}\sum_{n=1}^{\infty} \frac{W_{mn}^2(r_0,\theta_0)}{\left[\omega_{mn}^2(1+j\eta) - \omega^2\right] M_{mn}}. \tag{34}$$

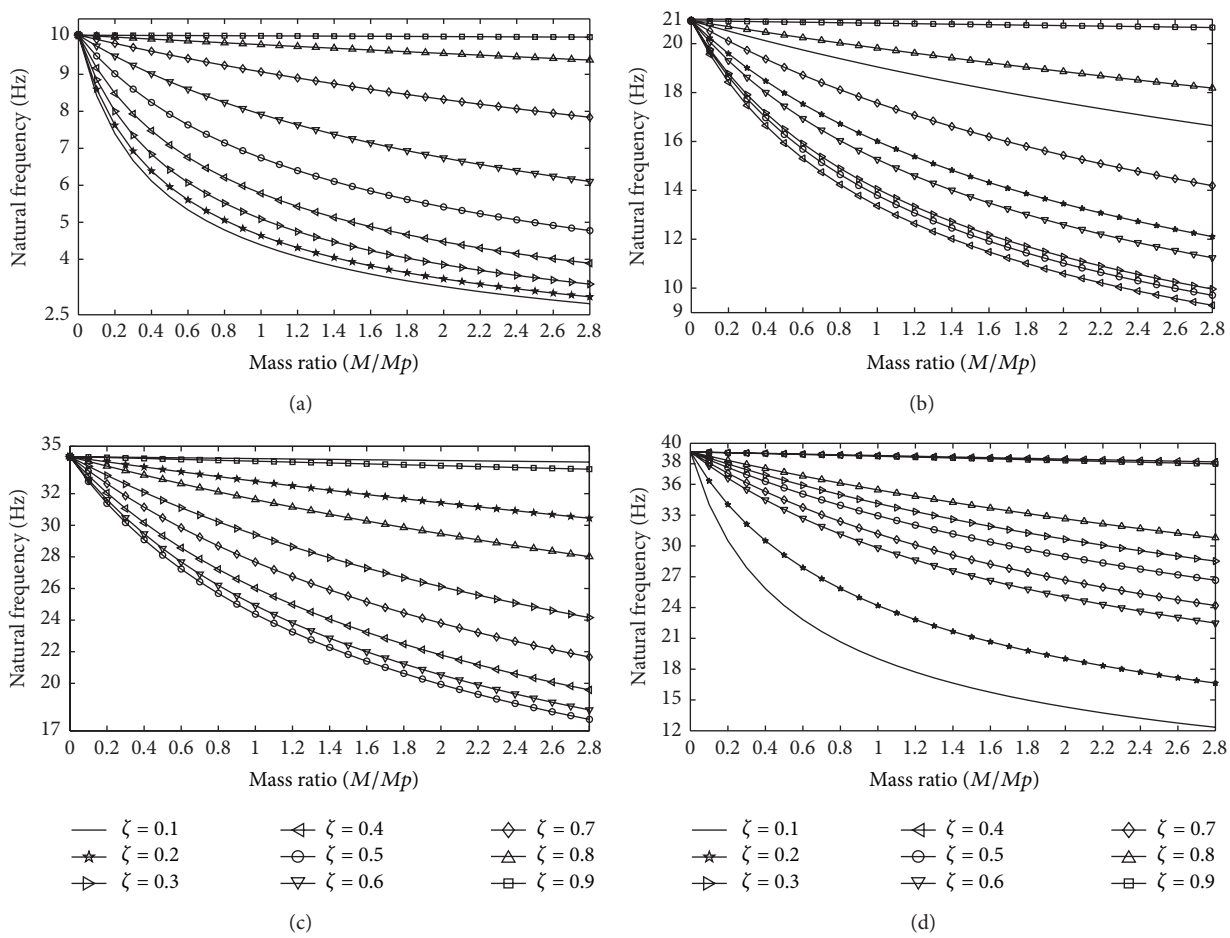

Figure 3: Lower 4 order natural frequencies of a clamped circular plate with a concentrated mass. (a) The 1st order natural frequency. (b) The 2nd order natural frequency. (c) The 3rd order natural frequency. (d) The 4th order natural frequency.

For the case of moment excitation, we may calculate the response at the excitation point P_0. The method used by Goyder and White [19] and Cremer et al. [3], departing the moment excitation into a pair of forces, a couple, composed of two opposite and equal forces applied at two points with a sufficiently small distance 2ε, was adopted. Hence, the moment M_x applied at (r_0, θ_0) can be replaced by two equal and opposite point forces, F and $-F$, applied at the positions $(r_0, \theta_0 + \varepsilon)$ and $(r_0, \theta_0 - \varepsilon)$, respectively. So, the resultant moment can be expressed as

$$M = 2\varepsilon F. \tag{35}$$

At the driving point, the force excitation does not generate a rotational velocity and the couple does not generate an out-of-plane velocity. Also, the rotational velocity at the driving point generated by the couple is in the same direction as that of the couple. Transverse displacement w and two rotations θ_x and θ_y can be observed based on Kirchhoff plate theory:

$$\theta_x = \frac{\partial w}{\partial y}, \tag{36a}$$

$$\theta_y = -\frac{\partial w}{\partial x}. \tag{36b}$$

The rotational velocity response of the plate subjected to the moment excitations M_x can then be obtained by summing the responses due to the excitation forces, F and $-F$, based on the superposition theorem for linear systems. The velocity response of the driving point P_0 can be represented as

$$\begin{aligned}\dot{\theta}_x(r_0, \theta_0) &= j\omega F \sum_{m=1}^{\infty}\sum_{n=1}^{\infty} \frac{\left[(\partial/\partial y) W_{mn}(r,\theta)\right]_{r_0\theta_0}}{\left[\omega_{mn}^2(1+j\eta) - \omega^2\right] M_{mn}} \\ &\quad \times \left[W_{mn}(r_0, \theta_0 + \varepsilon) - W_{mn}(r_0, \theta_0 - \varepsilon)\right].\end{aligned} \tag{37}$$

Therefore, the moment mobility functions could be given as

$$\begin{aligned}Y_{22} &= \frac{\theta_x(\dot{r}_0, \theta_0)}{M_x} \\ &= \frac{j\omega}{2\varepsilon} \sum_{m=1}^{\infty}\sum_{n=1}^{\infty} \frac{\left[(\partial/\partial y) W_{mn}(r,\theta)\right]_{r_0\theta_0}}{\left[\omega_{mn}^2(1+j\eta) - \omega^2\right] M_{mn}} \\ &\quad \times \left[W_{mn}(r_0, \theta_0 + \varepsilon) - W_{mn}(r_0, \theta_0 - \varepsilon)\right].\end{aligned} \tag{38}$$

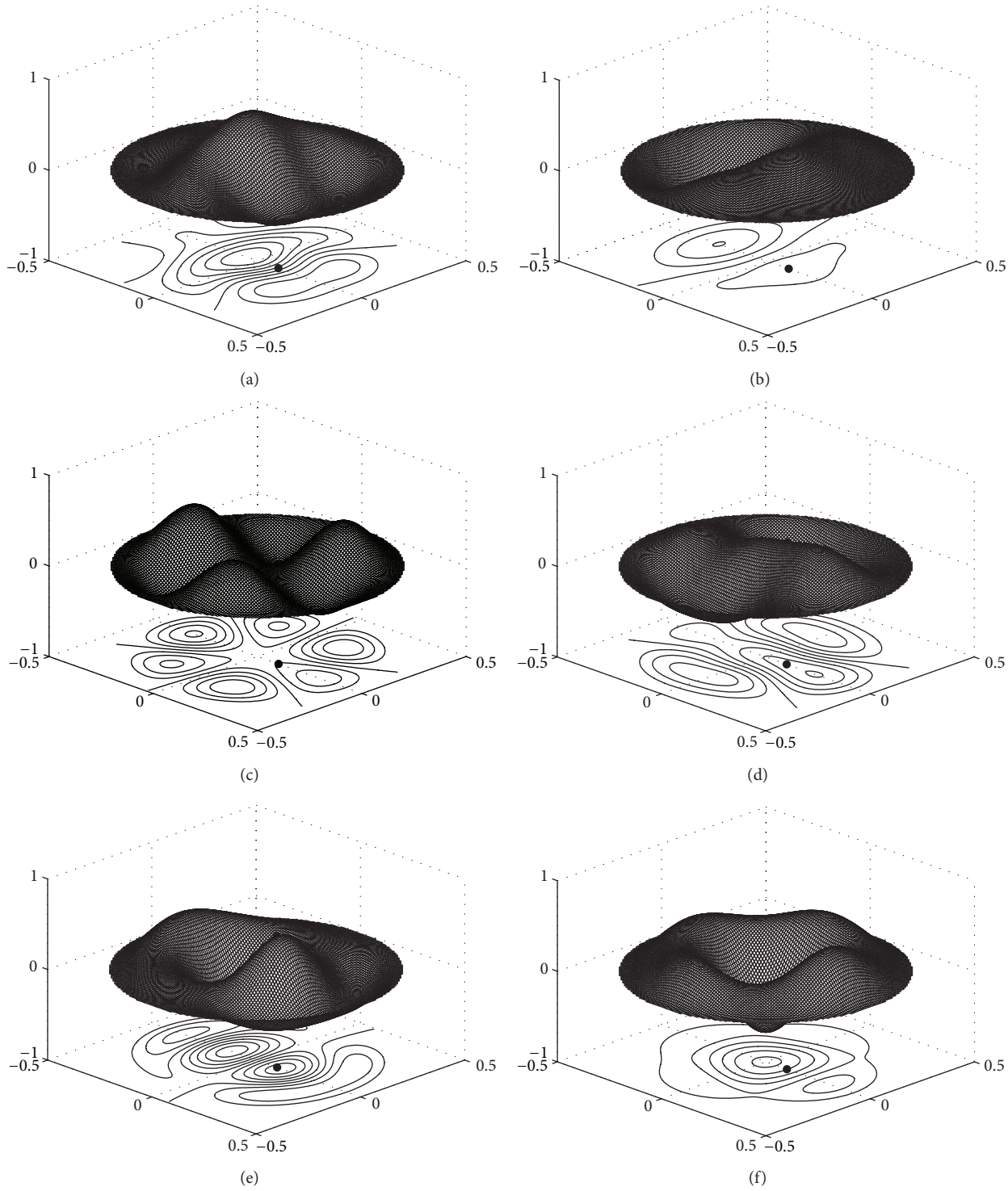

Figure 4: Lower 4 order natural modes of a clamped circular plate with a concentrated mass. (a) $\lambda_1^2 = 2.9403$, (b) $\lambda_2^2 = 12.9523$, (c) $\lambda_3^2 = 17.1266$, (d) $\lambda_4^2 = 34.5531$, (e) $\lambda_5^2 = 39.6482$, and (f) $\lambda_6^2 = 51.0152$.

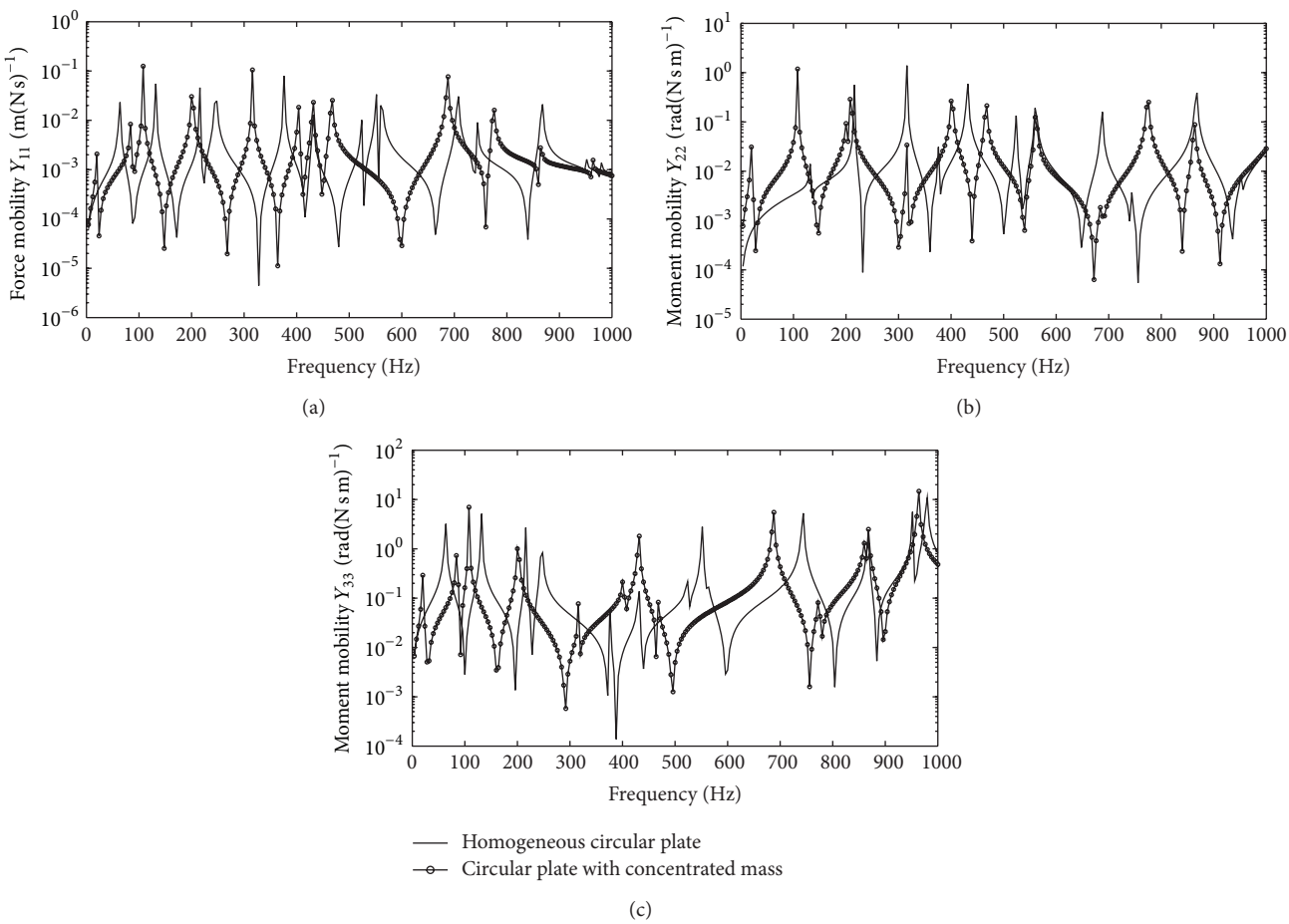

Figure 5: Modulus spectra of the driving force and moment mobility. (a) Force mobility Y_{11}. (b) Moment mobility Y_{22}. (c) Moment mobility Y_{33}.

In the other direction, y coordinate, the moment mobility Y_{33} could be obtained similarly.

The coupling mobility, the nondiagonal elements in (30), represents the functions between rotational DOF and the force excitation or translational DOF and the moment excitation. One can obtain them as

$$Y_{21} = \frac{\dot{\theta}_x(x_0, y_0)}{F}, \tag{39a}$$

$$Y_{31} = \frac{\dot{\theta}_y(x_0, y_0)}{F}, \tag{39b}$$

$$Y_{32} = \frac{\dot{\theta}_y(x_0, y_0)}{M_x}, \tag{39c}$$

$$Y_{12} = \frac{\dot{w}(x_0, y_0)}{M_x}, \tag{39d}$$

$$Y_{13} = \frac{\dot{w}(x_0, y_0)}{M_y}, \tag{39e}$$

$$Y_{23} = \frac{\dot{\theta}_x(x_0, y_0)}{M_y}. \tag{39f}$$

3.2. Transfer Point Mobility. The method outlined previously was extended to predict transfer point mobility, which is the complex ratio of the general velocity field generated at the receiving point P_1 to the general force field acts at the excitation point P_0 (see Figure 1). The transverse velocity generated at the point P_1 by a point transverse force at position P_0 is given by

$$\dot{w}(r_1, \theta_1) = j\omega F \sum_{m=1}^{\infty}\sum_{n=1}^{\infty} \frac{W_{mn}(r_1, \theta_1)}{[\omega_{mn}^2(1 + j\eta) - \omega^2] M_{mn}} W_{mn}(r_0, \theta_0). \tag{40}$$

Thus, the transfer force point mobility can be expressed as

$$Y_{11} = \frac{\dot{w}(r_1, \theta_1)}{F} = j\omega \sum_{m=1}^{\infty}\sum_{n=1}^{\infty} \frac{W_{mn}(r_1, \theta_1)}{[\omega_{mn}^2(1 + j\eta) - \omega^2] M_{mn}} W_{mn}(r_0, \theta_0). \tag{41}$$

Table 1: Comparison of fundamental frequency coefficients ${\lambda_1}^2 = \omega_1 a^2 \sqrt{\rho h/D}$ for a clamped circular plate with a concentrated mass at different positions ($\mu = 0.3$).

Position ratio r_M/a	Mass ratio M/M_p						
	0.1	0.2	0.3	0.5	1.0	1.5	2.0
0.1	8.5553	7.5074	6.7693	5.7751	4.4550	3.7586	3.3116
	[8.21]	[7.01]	[6.22]	[5.19]	[3.91]	[3.27]	[2.87]
	{8.1689}	{6.9397}	(6.060)	{5.0880}	{3.8136}	(3.140)	(2.748)
0.2	8.7274	7.7438	7.0320	6.0504	4.7114	3.9909	3.5241
	[8.45]	[7.34]	[6.58]	[5.56]	[4.25]	[3.57]	[3.14]
	{8.3265}	{7.1156}	(6.231)	{5.2394}	{3.9318}	(3.240)	(2.835)
0.3	8.9925	8.1243	7.4671	6.5228	5.1692	4.4131	3.9143
	[8.76]	[7.77]	[7.05]	[6.05]	[4.70]	[3.97]	[3.50]
	(8.517)	(7.354)	(6.531)	(5.453)	(4.098)	(3.418)	(2.992)
0.4	9.3144	8.6161	8.0545	7.1977	5.8699	5.0805	4.5425
	[9.12]	[8.27]	[7.61]	[6.64]	[5.24]	[4.46]	[3.95]
	(8.874)	(7.807)	(6.992)	(5.876)	(4.433)	(3.700)	(3.240)
0.5	9.6413	9.1540	8.7338	8.0423	6.8454	6.0613	5.4966
	[9.48]	[8.82]	[8.25]	[7.33]	[5.88]	[5.03]	[4.47]
	{9.3694}	{8.4964}	(7.655)	{6.5858}	{5.0107}	(4.138)	(3.626)
0.6	9.9162	9.6416	9.3887	8.9372	8.0433	7.3732	6.8467
	[9.82]	[9.39]	[8.96]	[8.17]	[6.70]	[5.77]	[5.13]
	(9.691)	(9.140)	(8.546)	(7.470)	(5.769)	(4.840)	(4.246)
0.7	10.0998	9.9877	9.8793	9.6727	9.2080	8.8044	8.4497
	[10.06]	[9.87]	[9.66]	[9.18]	[7.92]	[6.92]	[6.19]
	(9.970)	(9.757)	(9.489)	(8.811)	(7.151)	(6.059)	(5.334)
0.8	10.1887	10.1619	10.1353	10.0828	9.9549	9.8318	9.7131
	[10.18]	[10.14]	[10.10]	[9.99]	[9.61]	[9.04]	[8.39]
	(10.099)	(10.058)	(10.009)	(9.886)	(9.331)	(8.455)	(7.611)
0.9	10.2138	10.2118	10.2099	10.2060	10.1964	10.1868	10.1772
	[10.22]	[10.22]	[10.21]	[10.21]	[10.19]	[10.18]	[10.16]
	(10.132)	(10.130)	(10.127)	(10.121)	(10.106)	(10.088)	(10.065)

For the case of moment excitation at the driving point P_0, the rotational velocity generated at the receiving point P_1 can be derived by replacing the moment with a couple of transverse forces. According to Kirchhoff plate theory, as employed in Section 3.1, the rotational velocity response generated at point P_1 due to moment excitation M_x at the driving point P_0 can be derived by

$$\begin{aligned}\dot{\theta}_x(r_1,\theta_1) &= j\omega \frac{[\partial w(r,\theta)]_{r_1\theta_1}}{\partial y} \\ &= j\omega F \sum_{m=1}^{\infty}\sum_{n=1}^{\infty} \frac{[(\partial/\partial y) W_{mn}(r,\theta)]_{r_1\theta_1}}{[\omega_{mn}^2(1+j\eta)-\omega^2] M_{mn}} \\ &\quad \times [W_{mn}(r_0,\theta_0+\varepsilon) - W_{mn}(r_0,\theta_0-\varepsilon)].\end{aligned} \tag{42}$$

Therefore, the transfer moment mobility functions could be given as

$$\begin{aligned}Y_{22} &= \frac{\theta_x(\dot{r}_1,\theta_1)}{M_x} \\ &= \frac{j\omega}{2\varepsilon} \sum_{m=1}^{\infty}\sum_{n=1}^{\infty} \frac{[(\partial/\partial y) W_{mn}(r,\theta)]_{r_1\theta_1}}{[\omega_{mn}^2(1+j\eta)-\omega^2] M_{mn}} \\ &\quad \times [W_{mn}(r_0,\theta_0+\varepsilon) - W_{mn}(r_0,\theta_0-\varepsilon)].\end{aligned} \tag{43}$$

Unlike the situation of driving coupling mobility, the transfer coupling mobility has its own special characters. The force-moment excitation generates the rotational-transverse displacement at the receiving point, except the driving point. So the transfer coupling mobility matrix is not a symmetrical matrix.

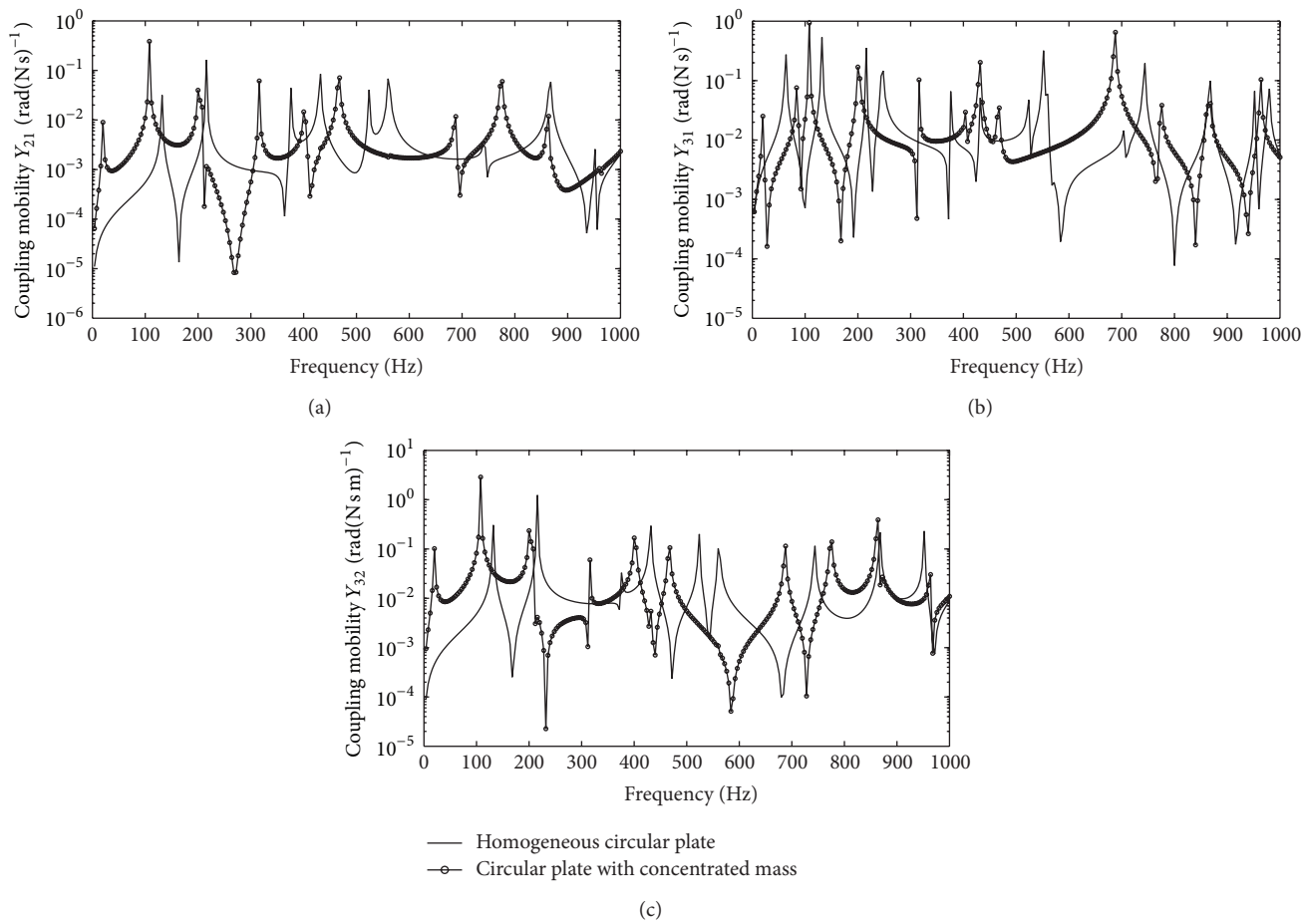

Figure 6: Modulus spectra of the driving coupling mobility. (a) Coupling mobility Y_{21}. (b) Coupling mobility Y_{31}. (c) Coupling mobility Y_{32}.

4. Example Applications

This section presents the calculated transverse vibration and the mobility results of a clamped circular plate carrying a concentrated mass. Comparisons are made with those existing and available to validate the method, based on which to predict its driving and transfer point mobility matrices.

4.1. Transverse Vibration. Figure 3 is the lower 4 order frequencies of a clamped circular plate with a concentrated mass at various positions. The plots present how the frequency curves decrease as the mass ratio increases from 0 to 2.8 and the position ratio from 0 to 0.9 as it was to be expected.

The natural frequency curves of each order distribute regularly. It can be observed from the 1st order that the variation of natural frequency is more noticeable when the mass is near to the center $\varsigma = 0.1$ of the plate than close to the outer boundary $\varsigma = 0.9$. It can be found from the 2nd order that the most sensitive position ratio is not $\varsigma = 0.1$ but $\varsigma = 0.4$. For the 3rd order, the position ratio $\varsigma = 0.1$ appears as the most insensitive parameter dramatically and meanwhile the most sensitive position ratio turns to be $\varsigma = 0.5$. For the 4th order, the most insensitive parameter is the position ratio $\varsigma = 0.4$ together with $\varsigma = 0.9$ while the most sensitive parameter is the position ratio $\varsigma = 0.1$.

Comparison with the numerical results of the natural frequency in [21] could validate the correctness and accuracy of the mathematical model presented in this paper.

Table 1 is the calculated fundamental frequency coefficients. Comparison with the published results available for the clamped thin isotropic circular plate with a concentrated mass is performed. Values in round brackets are cited from [22], in square brackets from [21], and in curly brackets from [23]. It is found that the results obtained by the present approach correlate well with the 1st natural frequency in Figure 3(a). The main reason for the data in Table 1 being slightly higher than those in the literatures is that the derivation calculation of the Bessel functions in (17a)–(17d) generates truncation error when performed via the recurrence formula.

Figure 4 is the lower 6 order vibration modes of clamped case with a concentrated mass whose mass ratio is 2.6 and position is $(0.2a, 0)$. It can be seen from the plots that the nodal diameters and nodal circles were changed into the nodal segments and nodal arcs under the effect of the concentrated mass. In addition, the concentrated mass generates the local wave crest and wave trough, which could be observed from the contours of the mode shapes.

4.2. Driving Point Mobility. Figures 5 and 6 are the modulus spectra of six-driving-point mobility of the clamped circular

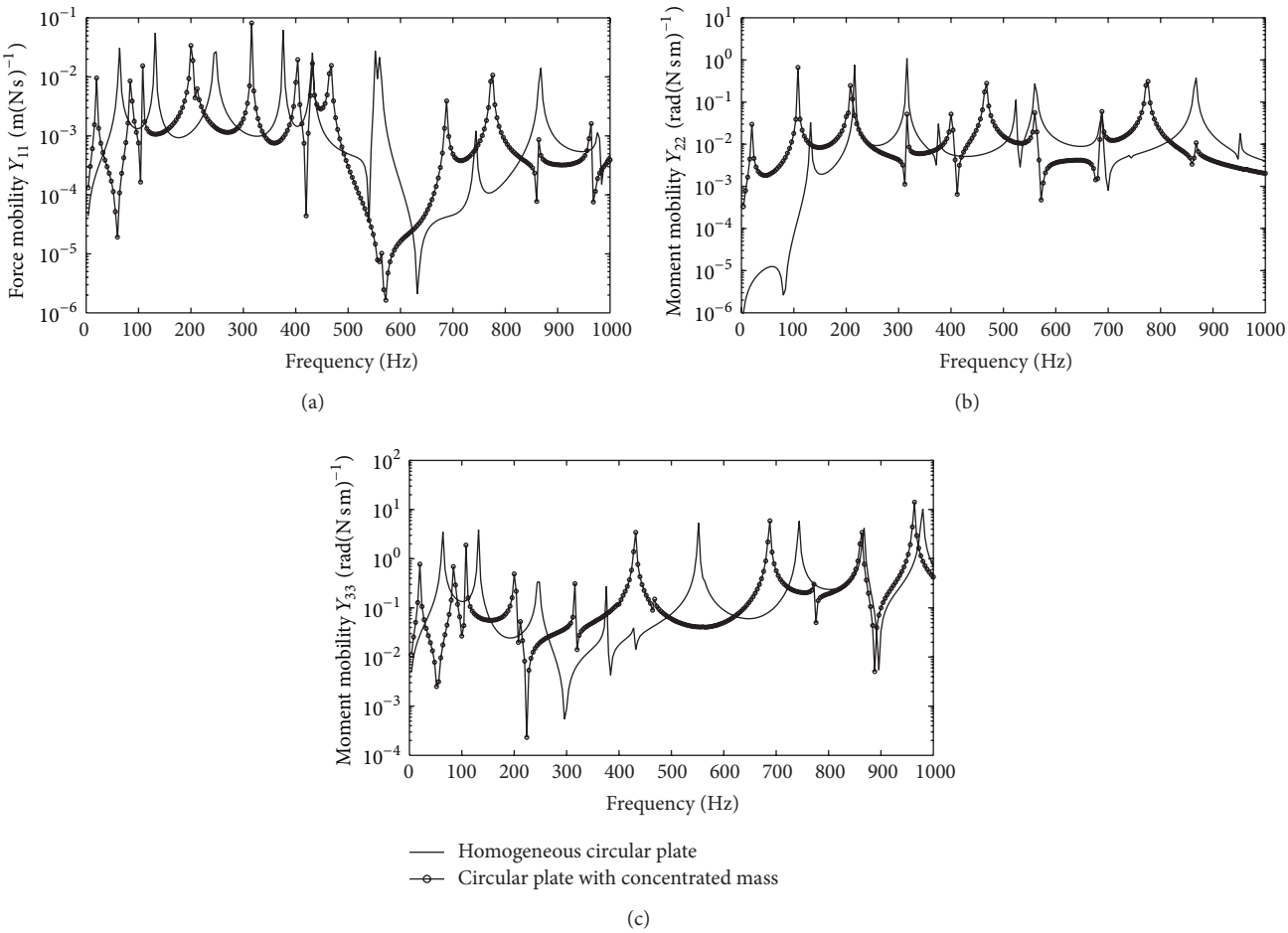

Figure 7: Modulus spectra of the transfer force and moment mobility. (a) Force mobility Y_{11}. (b) Moment mobility Y_{22}. (c) Moment mobility Y_{33}.

plate carrying a concentrated mass, whose mass ratio is 2.6 and position is $(0.2a, 0)$. The simple harmonic force and moment excitation with unite amplitude act at the point $(0.75a, 5\pi/6)$. The thickness and the radius of the plate are 1×10^{-3} m and 0.5 m. The elastic modulus, density, loss factor, and Poisson ratio are $2.05 \times 10^{11}\,\mathrm{Nm}^{-2}$, $7.85 \times 10^{3}\,\mathrm{kgm}^{-3}$, 0.001, and 0.3, respectively. The mobility of the same plate with no concentrated mass is also given.

It can be seen from Figure 5 that the concentrated mass has an obvious effect on the driving point mobility. Relative to the homogeneous case, more resonance peaks emerge in the force and moment mobility plots, such as the local tiny peaks at 97 Hz in plot (a), 212 Hz and 698 Hz in (b), and 782 Hz in (c).

Lots of major peaks slide toward to the lower frequency band more or less, as can be seen in Figure 6. The peak generated at 860 Hz in plot (a) for homogeneous circular plate appears at 782 Hz in advance when it comes to the case of concentrated mass. The same situations could also be found in the other coupling mobility. For example, the peak is from 840 Hz to 801 Hz and from 198 Hz to 167 Hz in plot (b) and from 675 Hz to 590 Hz in plot (c). The reason for the peaks slide toward lower frequency band is that the concentrated mass reduced the structure's natural frequency, which corresponds to the major peaks.

For a linear system, the driving point mobility matrix is symmetric; thus the coupling mobility functions between the translational velocity and the moment excitation, that is, Y_{12} and Y_{13}, equal the coupling mobility functions between the rotational velocity and the force excitation, that is, Y_{21} and Y_{31}, respectively. The coupling mobility functions between the rotational velocity and the moment excitation, that is, Y_{32} and Y_{23}, are equal to each other because of the isotropic medium of the plate. Specifically, the coupling mobility is zero when the plate center was taken as the driving point.

4.3. Transfer Point Mobility. Figures 7 and 8 are the transfer mobility of the same structure in Section 4.2. The transfer path is from the excitation point P_0 $(0.75a, 5\pi/6)$ to the resultant velocity point P_1 $(0.65a, -\pi/4)$; see Figure 1. As with the situation of driving mobility, concentrated mass has a significant effect on transfer point mobility. Figure 7 is the transfer force and moment mobility of the circular plate with concentrated mass. It shows that the transfer moment mobility Y_{22} has a numerical increase sharply at the frequency

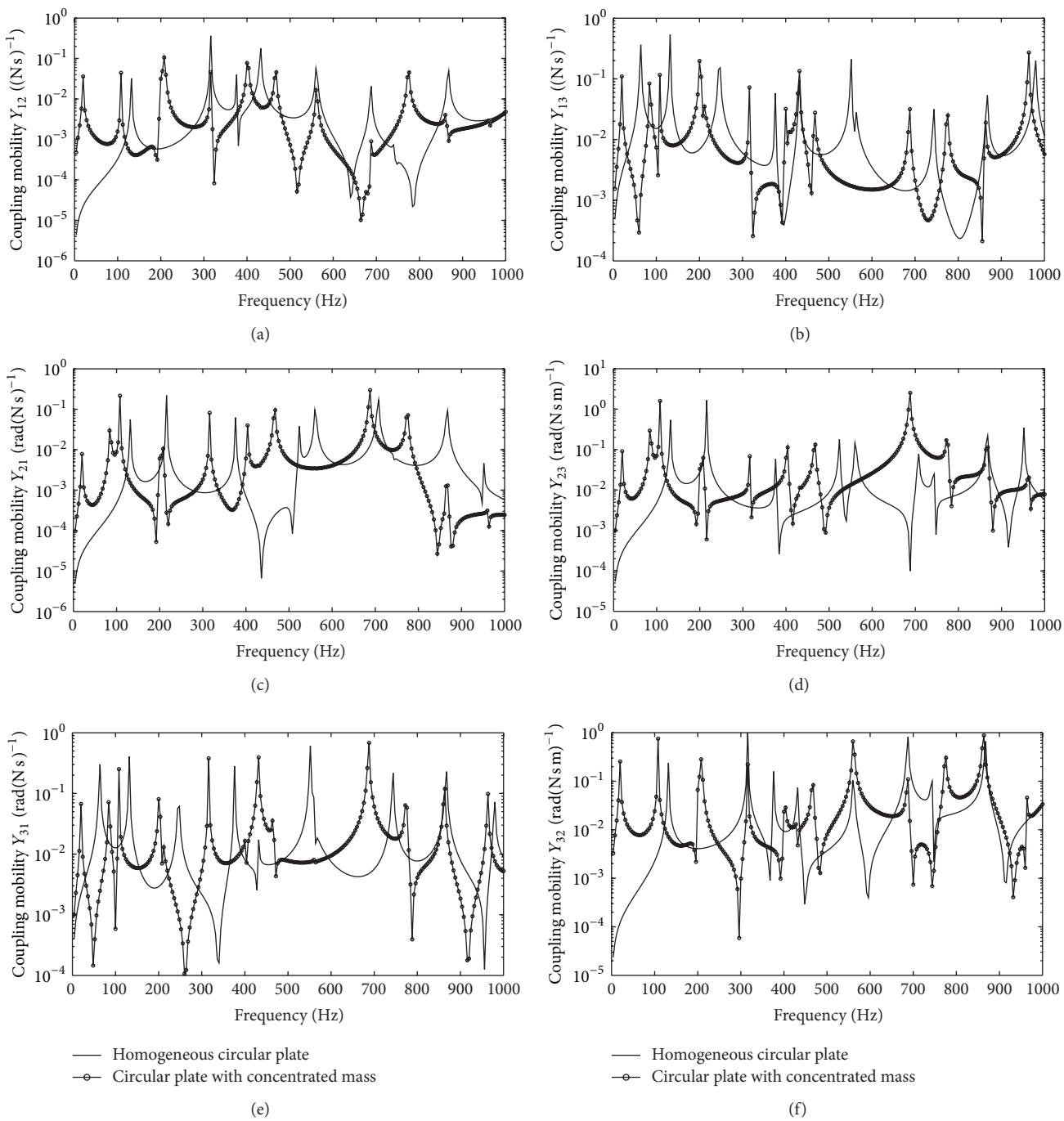

Figure 8: Modulus spectra of the transfer coupling mobility. (a) Coupling mobility Y_{12}. (b) Coupling mobility Y_{13}. (c) Coupling mobility Y_{21}. (d) Coupling mobility Y_{23}. (e) Coupling mobility Y_{31}. (f) Coupling mobility Y_{32}.

band below 110 Hz in contrast to the case of homogeneous plate. For the force mobility Y_{11} and moment mobility Y_{33}, the criticality frequency value is about 30 Hz, in which the peaks appear in advance because of the reduction of the natural frequency. For the moment mobility Y_{33}, plot (c) shows that the concentrated mass has less effect almost in the frequency band above 840 Hz.

Figure 8 is the transfer coupling mobility on which the effect of the concentrated mass is similar to the force and moment mobility in Figure 7. The different types of coupling mobility Y_{12}, Y_{21}, Y_{23}, and Y_{32} have a numerical increase sharply at the frequency band below 110 Hz in contrast to the homogeneous case. For the two types of coupling mobility Y_{13} and Y_{31}, about 30 Hz is a threshold value below which the coupling mobility of the plate with concentrated mass is higher than that of homogeneous case.

4.4. Application of Point Mobility. This section presents the transverse vibration response by using the point mobility of

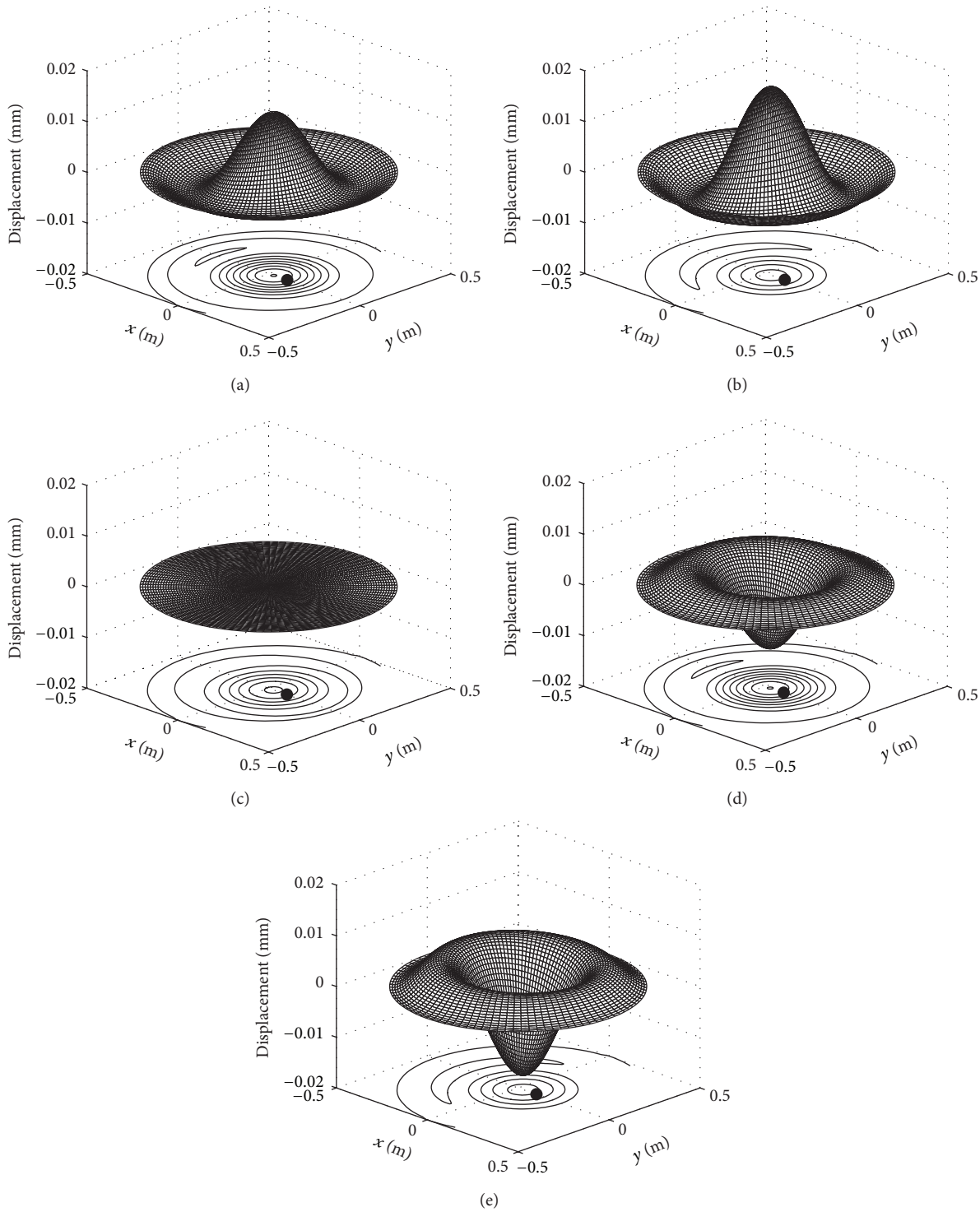

Figure 9: Displacement response at various moments in a completely periodicity T. (a) $t = T/8$ (3T/8), (b) $t = T/4$,(c) $t = T/2$ (T), (d) $t = 5T/8$ (7T/8), and (e) $t = 3T/4$.

the clamped circular plate with a concentrated mass, which mass ratio is 2.6 and position is $(0.2a,\ 0)$ in polar coordinate system. Considering the out-of-plane excitation force which is $F = 100\sin(50\pi t)$ N acts at the plate center, the transverse displacement response at various moments in a completely periodicity T can be obtained as shown in Figure 9. Figure 10 is the displacement of points 1 and 2, which positions are $(0.5a, \pi)$ and $(0.8a, \pi)$, respectively. It can be observed from

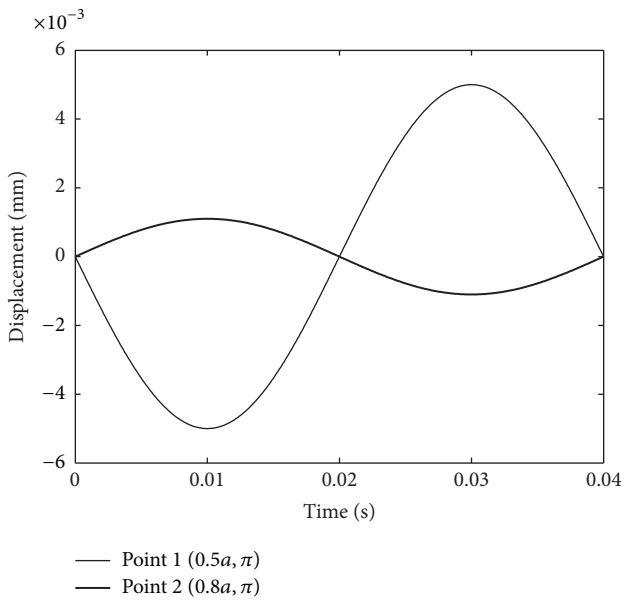

Figure 10: Displacement response of the points 1 and 2.

the plots that the response of the plate is a simple harmonic motion, whose periodicity is the same with the excitation force.

5. Conclusions

This work is related to how to compute the driving and transfer point mobility matrix of a concentrated mass-loaded circular plate. Firstly, a new mathematical model based on the structural circumferential periodicity of inertia excitation produced by the concentrated masses was presented to solve the transverse free vibration characteristics. The numerical results, including the natural frequency and fundamental frequency coefficient, of the clamped case were compared to the published ones to validate the present method and to ensure the correctness of mobility solution. Furthermore, the driving and transfer point mobility matrices were calculated based on the analytical mode functions solution and the effect of the concentrated mass on the point mobility was analyzed. The main findings from the study are as follows.

(1) For the driving point mobility, concentrated mass generates more resonance peaks in force and moment point mobility in contrast to the homogeneous case. This situation corresponds well with the local wave crests and wave troughs in the mode shapes. For the coupling mobility, the major wave crest slides toward the lower frequency band due to the concentrated mass.

(2) The transfer point mobility, including the force, moment, and coupling mobility, has a numerical sharp increase in the frequency band below 110 Hz and the wave crests emerge in advance because of the natural frequency decreases due to the concentrated masses.

(3) The driving point mobility matrix of concentrated mass-loaded circular plate is symmetric because the mass does not change the linearity of the system. Specially, the nondiagonal elements are zeros if the plate center was taken as the driving point. For transfer point mobility, the mobility matrix is not symmetric.

Conflict of Interests

The authors declare that there is no conflict of interests regarding the publication of this paper.

Acknowledgments

The authors would like to gratefully acknowledge the support of this research by National High Technology Research and Development Program (no. 2012AA1117064) and the Project supported by Technology Research of Engine Vibration and Noise Control.

References

[1] F. Fahy, *Foundations of Engineering Acoustics*, Academic Press, Oxford, UK, 2000.

[2] F. Fahy and P. Gradonio, *Sound and Structural Vibration: Radiation, Transmission and Response*, Academic Press, Oxford, UK, 2nd edition, 2007.

[3] L. Cremer, M. Heckl, and E. E. Ungar, *Structure-Borne Sound*, Springer, Berlin, Germany, 2nd edition, 1988.

[4] E. Sarradj, "Calculation of point mobilities at generic multi-plate/beam junctions," *Journal of Sound and Vibration*, vol. 229, no. 2, pp. 411–430, 2000.

[5] A. T. Moorhouse and B. M. Gibbs, "Calculation of the mean and maximum mobility for concrete floors," *Applied Acoustics*, vol. 45, no. 3, pp. 221–245, 1995.

[6] H. A. Bonhoff and B. A. T. Petersson, "The influence of cross-order terms in interface mobilities for structure-borne sound source characterization: plate-like structures," *Journal of Sound and Vibration*, vol. 311, no. 1-2, pp. 473–484, 2008.

[7] A. R. Mayr and B. M. Gibbs, "Point and transfer mobility of point-connected ribbed plates," *Journal of Sound and Vibration*, vol. 330, no. 20, pp. 4798–4812, 2011.

[8] B. A. T. Petersson and M. Heckl, "Concentrated excitation of structures," *Journal of Sound and Vibration*, vol. 196, no. 3, pp. 295–321, 1996.

[9] D. Sciulli, *Dynamics and control for vibration isolation design [Ph.D. dissertation]*, Virginia Polytechnic Institute and State University, 1997.

[10] R. M. Grice and R. J. Pinnington, "Analysis of the flexural vibration of a thin-plate box using a combination of finite element analysis and analytical impedances," *Journal of Sound and Vibration*, vol. 249, no. 3, pp. 499–527, 2002.

[11] A. Putra, *Sound radiation from perforated plates [Ph.D. thesis]*, University of Southampton, Southampton, UK, 2008.

[12] B.-T. Wang, "Vibration analysis of a continuous system subject to generic forms of actuation forces and sensing devices,"

Journal of Sound and Vibration, vol. 319, no. 3-5, pp. 1222–1251, 2009.

[13] Y. Yun and C. M. Mak, "Power transmission from two coherent machines to a dual-layer coupling floor structure," *Journal of Vibration and Control*, vol. 17, no. 5, pp. 711–720, 2011.

[14] F. Zu and C. M. Mak, "Estimation of best mounting positions for vibratory equipment in buildings," *Journal of Vibration and Control*, vol. 17, no. 2, pp. 301–310, 2011.

[15] X. Huang, S. Xu, A. Jiang, and H. Hua, "Modeling and optimization of floating raft systems in submarines under different objectives by using hybrid genetic algorithm," *Journal of Vibration and Control*, vol. 18, no. 2, pp. 268–297, 2012.

[16] R. Chen and T. Wu, "Vibration control of base system using distributed dynamic vibration absorbers," *Journal of Vibration and Control*, 2013.

[17] M. Shariyat and M. M. Alipour, "A power series solution for vibration and complex modal stress analyses of variable thickness viscoelastic two-directional FGM circular plates on elastic foundations," *Applied Mathematical Modelling*, vol. 37, no. 5, pp. 3063–3076, 2013.

[18] E. P. Bowyer, D. J. O'Boy, V. V. Krylov, and F. Gautier, "Experimental investigation of damping flexural vibrations in plates containing tapered indentations of power-law profile," *Applied Acoustics*, vol. 74, no. 4, pp. 553–560, 2013.

[19] H. G. D. Goyder and R. G. White, "Vibrational power flow from machines into built-up structures. Part I: introduction and approximate analyses of beam and plate-like foundations," *Journal of Sound and Vibration*, vol. 68, no. 1, pp. 59–75, 1980.

[20] A. W. Leissa, *Vibration of Plates*, vol. 160 of *NASA SP*, National Aeronautics and Space Administration, 1969.

[21] D. V. Bambill, S. La Malfa, C. A. Rossit, and P. A. A. Laura, "Analytical and experimental investigation on transverse vibrations of solid, circular and annular plates carrying a concentrated mass at an arbitrary position with marine applications," *Ocean Engineering*, vol. 31, no. 2, pp. 127–138, 2004.

[22] V. Ranjan and M. K. Ghosh, "Transverse vibration of thin solid and annular circular plate with attached discrete masses," *Journal of Sound and Vibration*, vol. 292, no. 3–5, pp. 999–1003, 2006.

[23] S. Maiz, C. A. Rossit, D. V. Bambill, and A. Susca, "Transverse vibrations of a clamped elliptical plate carrying a concentrated mass at an arbitrary position," *Journal of Sound and Vibration*, vol. 320, no. 4-5, pp. 1146–1163, 2009.